Interaction and ordering of vacancy defects in NiO

Sohee Park,[1] Hyo-Shin Ahn,[1] Choong-Ki Lee,[1] Hanchul Kim,[4] Hosub Jin,[2] Hyo-Sug Lee,[3] Sunae Seo,[3] Jaejun Yu,[2] and Seungwu Han[1,*]

[1]*Department of Physics, Ewha Womans University, Seoul 120-750, Republic of Korea*

[2]*School of Physics and CSCMR, Seoul National University, Seoul 151-747, Korea*

[3]*Samsung Advanced Institute of Technology, Suwon 440-600, Korea*

[4]*Korea Research Institute of Standards and Science, P.O. Box 102, Yuseong, Daejeon 305-600, Korea*

(Received 11 February 2007; revised manuscript received 25 December 2007; published 7 April 2008)

By using a first-principles method employing the local density approximation plus Hubbard parameter approach, we study point defects in NiO and interactions between them. The defect states associated with nickel or oxygen vacancies are identified within the energy gap. It is found that nickel vacancies introduce shallow levels in the density of states for the spin direction opposite to that of the removed Ni atom, while the oxygen vacancy creates more localized in-gap states. The interaction profiles between vacancies indicate that specific defect arrangements are strongly favored for both nickel and oxygen vacancies. In the case of nickel vacancies, defect ordering in a simple-cubic style is found to be most stable, leading to a half-metallic behavior. The ionized oxygen vacancies also show a tendency toward clustering, more strongly than neutral pairs. The microscopic origin of vacancy clustering is understood based on overlap integrals between defect states.

DOI: 10.1103/PhysRevB.77.134103 PACS number(s): 71.55.−i, 71.15.Mb

I. INTRODUCTION

Vacancies at anion or cation sites in insulating transition-metal oxides often give rise to the generation of charge carriers or conducting channels, thereby profoundly affecting transport properties of the host material.[1] To clarify how vacancy defects modify the electronic structures of materials, various experimental and theoretical efforts are employed, but it is a challenging task to distinguish vacancy-related properties from those that originate from other types of defects. The situation becomes even more complicated in the case of nonstoichiometric oxides with higher densities of the vacancy; the vacancy-vacancy interaction can trigger a certain type of defect ordering by overcoming entropic penalties. As an example, oxygen vacancies in highly reduced barium titanate ($BaTiO_3$) were found to be ordered in a superstructure.[2] As the experimental techniques are developed to control compositional ratios within the materials, the importance of vacancy clusters has been greatly increased.[3]

In this work, we carry out first-principles studies on vacancy defects in nickel oxide (NiO) with isolated or associated forms. NiO has been extensively studied to understand correlation effects of localized *d* electrons. The origin of insulating behaviors has been debated, and it is now widely accepted that NiO is a charge-transfer-type insulator.[4] NiO shows a *p*-type conductivity with hole carriers generated by cation vacancies. Despite their importance to the transport properties, point defects in NiO have been rarely studied using theoretical approaches,[5] leading to the dearth of microscopic pictures of vacancy structures. Our interests in NiO stem partly from a recent application to a nonvolatile memory, which exploits resistance switching behaviors of NiO.[6] Although the underlying mechanism of resistance switching is yet to be unraveled, it is likely that defects play a central role in bistable resistance properties.[7]

The electron correlation in NiO requires a theoretical framework that goes beyond the conventional local density approximation (LDA). Previous studies show that the electronic structure of NiO is strongly affected by the on-site Coulomb interaction between electrons occupying Ni *d* orbitals. LDA suffers from the inherent self-interaction, which substantially affects the energy levels associated with the localized orbital. There are several methods that are capable of overcoming the limitation of LDA; GW method,[8] self-interaction correction (SIC),[9] pseudo-SIC,[10] Hartree–Fock,[11] cluster approach based on the configuration interactions,[12,13] hybrid density functionals,[14] and LDA+U method.[15–17] Among them, the LDA+U method is computationally efficient with a moderate increase of the computational costs from conventional density functional calculations, although the inherent empirical parameters necessitate further validation. The LDA+U method has been applied to understand the bulk properties of NiO,[15–17] the electronic structures of NiO surfaces,[18] and their interactions with small molecules.[17] Insofar as we are aware, this method has not been employed for studying defect properties of NiO. In this work, we identify defect states in NiO induced by vacancies and show that their spatial distributions are detrimental to defect associations, possibly leading to a spatial ordering. Furthermore, it is found that orbital symmetries as well as detailed electronic structures are crucial in the determination of the electronic structures in NiO related to defects. This result may shed light on the understanding of electronic structures and interactions of vacancy defects in other transition-metal oxides, such as CoO or $BaTiO_3$. This paper is organized as follows: In Sec. II, the computational setup is outlined. Computational results and discussions are given in Sec. III, and main achievements are summarized in Sec. IV.

II. COMPUTATIONAL METHODS

For first-principles calculations, we use a computational code of Vienna *ab initio* simulation package (VASP).[19] The

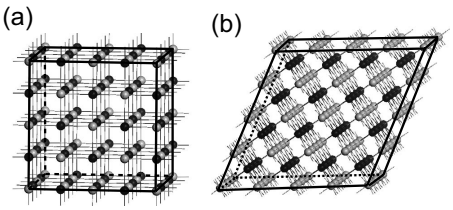

FIG. 1. Supercell geometries used for calculating defect properties. (a) A simple-cubic style supercell with the f.u. of $Ni_{32}O_{32}$. (b) A face-centered-cubic (fcc) supercell ($Ni_{64}O_{64}$) is obtained by expanding the lattice vectors of fcc unit cell twice along each direction. The lengths of lattice vectors in (a) and (b) are 8.38 and 11.85 Å, respectively. The black and gray spheres indicate oxygen and nickel atoms, respectively.

interactions between electrons and ions are described by projector-augmented-wave potentials.[20] The valence configurations are $3d^84s^2$ and $2s^22p^4$ for Ni and O atoms, respectively. The exchange and correlation energies of electrons are described within the spin-polarized generalized gradient approximation (SGGA) with a functional form proposed in Ref. 21. The plane waves with an energy cutoff of 400 eV are used for expanding electronic wave functions. For the *k*-point integration, $4\times4\times4$ and $2\times2\times2$ regular meshes are used for simple-cubic and face-centered-cubic supercells containing 64 and 128 atomic sites, respectively (see below). To test the convergence, we increase the energy cutoff up to 600 eV and the *k*-point mesh up to $6\times6\times6$ in the 64-atom supercell and find that atomic relaxations and defect formation energies change by less than 0.01 Å and 0.01 eV, respectively. The density of states (DOS) is broadened with a Gaussian function with a width of 0.02 eV. The atomic positions are relaxed until the Hellmann–Feynman force on each atom is reduced to within 0.05 eV/Å. As mentioned above, the electronic correlation effects in NiO need an explicit description of on-site Coulomb interactions associated with Ni *d* electrons. We employ SGGA+*U* methods as implemented within the code. We use 6.3 and 1.0 eV for *U* and *J* parameters, indicating the on-site screened Coulomb energy and exchange interactions, respectively. This follows a recipe given in Ref. 17 where extensive calculations were performed to test parameters. We employ the rotationally invariant form of the SGGA+*U* functional in Ref. 15; therefore, the model Hamiltonian describing the on-site interaction depends only on *U-J*.

For calculating point defects within the periodic boundary conditions, we adopt supercells that are compatible with the type-II antiferromagnetic structure of NiO (see below). We consider two types of the supercell geometry, as displayed in Fig. 1. The smaller one is a simple-cubic cell containing 64 atoms ($Ni_{32}O_{32}$). A larger supercell is obtained by expanding face-centered-cubic unit cells of NiO twice along each lattice vector, and it contains 128 atoms ($Ni_{64}O_{64}$).

III. RESULTS AND DISCUSSIONS

A. Bulk properties

We first calculate on the structural and electronic properties of crystalline NiO in type-II antiferromagnetic ordering.

TABLE I. Computational results on the bulk properties of NiO. Lattice parameters (a_0), bulk modulus (B_0), magnetic moment at Ni sites (m), minimum energy gap (E_g^{CT}), and optical gap (E_g^{op}) are shown. The magnetic moment is obtained by projecting the spin density onto *d* orbitals of Ni atoms. Other experimental and theoretical results are also shown for comparison.

		Other theories		
	This work	LSDA+U[a]	SGGA+U[b]	Experiment[c]
a_0 (Å)	4.19	4.07, 4.19	4.20	4.17
B_0 (GPa)	189	236, 182	202.5	205
m (μ_B)	1.67	1.59, 1.64	1.72, 1.7	1.9
E_g^{CT} (eV)	2.96			
E_g^{op} (eV)	3.53	3.1, 3.0	3.2, 2.7	3.7-4.3

[a]References 15, 17, and 22.
[b]References 17 and 23.
[c]References 15 and 24–29.

Type-II ordering means that the spin moments of Ni atoms within the same (111) plane are ferromagnetically aligned with the spin direction alternating between neighboring planes. The results are compiled in Table I, together with previous experimental and theoretical data for a comparison purpose. The overall agreements with previous literatures are satisfactory. To compare stability between different magnetic orderings, we also calculate on ferromagnetic or type-I antiferromagnetic NiO. In a type-I antiferromagnetic phase, the ordering vector is along (100). The equilibrium lattice parameters are computed to be 4.21 Å for both cases, slightly longer than that of NiO in the type-II ordering. The calculated total energies indicate that ferromagnetic and type-I antiferromagnetic phases are higher in energy than the type-II phase by 0.11 and 0.12 eV/f.u. of NiO, respectively. In Fig. 2, partial DOS is shown by projecting each state onto atomic orbitals. It is found that the valence top is a hybridized character between Ni t_{2g} and O *p* orbitals, while the conduction bottom is mainly composed of Ni e_g orbitals in spin minority, indicating that the band gap is a charge-transfer type.

B. Properties of point defects

1. Single nickel vacancy

Under a typical growth condition, NiO is deficient with cations, which explains *p*-type conducting behaviors.[1] We

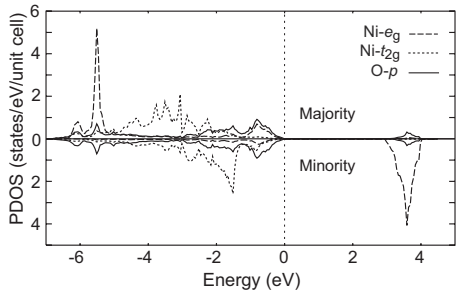

FIG. 2. Partial DOS of NiO in type-II antiferromagnetic ordering. The Fermi level is set to zero (vertical dotted line).

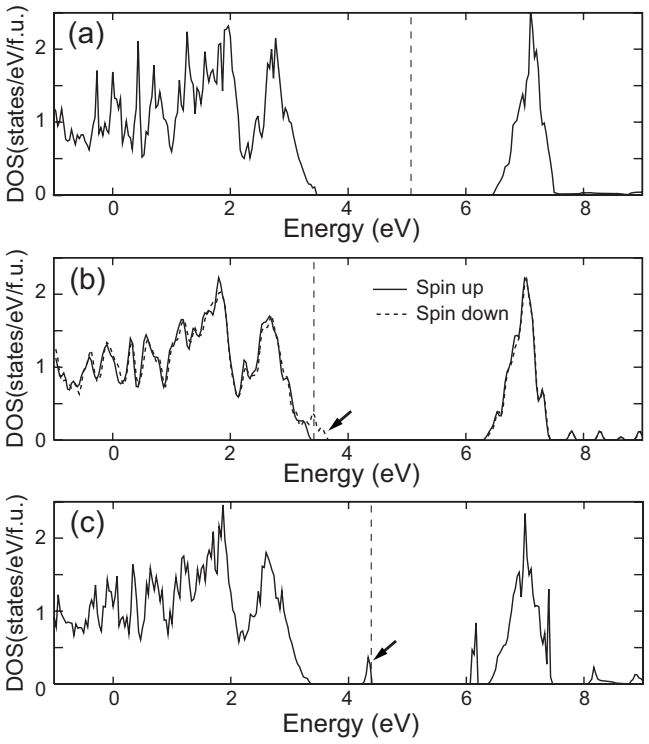

FIG. 3. The total density of states (TDOS) of crystalline and defective NiO. (a) TDOS of defect-free NiO in type-II antiferromagnetic ordering. (b) TDOS of $Ni_{63}O_{64}$, including one vacancy at the Ni site with an up-spin direction. (c) TDOS of $Ni_{32}O_{31}$ with one oxygen vacancy. The Fermi levels are indicated by vertical dashed lines. For comparison between structures with different numbers of atoms, DOS is divided by the number of f.u.

note that the nickel vacancy (V_{Ni}) in a real situation can be filled with other impurity atoms, such as Fe or Li. In order to study single V_{Ni}, we use a face-centered-cubic supercell including 128 atoms shown in Fig. 1(b) and remove one Ni atom with a spin-up direction. The relaxation pattern shows that nearby oxygen atoms around the defect site relax outward by 0.17 Å. This can be explained based on the electrostatic interaction between the defect site and nearby atoms; with loosely bound holes (see below), the effective charge of V_{Ni} is negative, which is identical to those of oxygen atoms. Therefore, oxygen atoms are repelled from the defect site, accounting for the relaxation pattern.

In Fig. 3(b), the total DOS is shown in the presence of single V_{Ni}. For comparison, the DOS for crystalline NiO is also shown in Fig. 3(a). The electronic structure indicates a half-metallic property; i.e., only one spin channel is metallic. The holes are created in the down spin that is opposite to the spin direction of the removed Ni atom. A similar observation was reported in Ref. 5. In real situations, however, nickel vacancies at diluted limits are randomly distributed throughout the material. Therefore, DOS would be nearly symmetric for both spin directions, canceling out the half-metallic property. This can be changed when one considers defect clustering, which will be discussed in Sec. III C. From the analysis on the partial DOS (not shown), it is found that holes are of a mixed character of Ni d and O p orbitals in six oxygen and

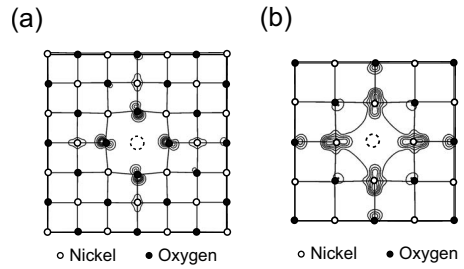

FIG. 4. The squared wave function of defect states indicated by arrows in Figs. 3(b) and 3(c). (a) The defect level at the valence top in the presence of the nickel vacancy [see Fig. 3(b)]. (b) The in-gap state created by the oxygen vacancy in Fig. 3(c). The charge densities are added over the spin directions.

nickel atoms that are closest to the defect site along six bonding directions. This is consistent with Fig. 4(a), which shows a contour plot of the squared wave function sampled near the valence maximum (down spin). It can be seen that the wave function is localized noticeably at six oxygen and nickel atoms along the bonding directions. This is due to the superexchange interaction between Ni d orbitals mediated by O p orbitals. As a result, the coupling between second nearest neighbor (NN) Ni atoms is much larger than those between the first NN pairs. This is in line with the scanning-tunneling-microscope image obtained from the Ni defect on the NiO(001) surfaces.[30,31] The majority spin of Ni atoms at the second NN sites from the defect is along the down direction; therefore, the creation of holes in the spin-down channel reduces the magnetic moments of these Ni atoms to $1.45\mu_B$ as compared to $1.67\mu_B$ in the bulk (see Table I). The binding energy of the hole at the nickel vacancy can be estimated from the energy difference between the center of defect bands (first moment) and the valence edge. From the inspection of the band structure, we find a binding energy of ~0.2 eV. This is in good comparison with an experimental activation barrier of 0.3 eV reported in Ref. 32 although a correlated hopping model proposed in the work is not born out within the SGGA+U framework.

2. Single oxygen vacancy

Although the cation vacancy is known to be a major point defect in bulk NiO, the growth condition with low oxygen pressures may result in appreciable concentrations of the oxygen vacancy (V_O). For calculating the oxygen vacancy, a cubic supercell with 64 atoms is used [see Fig. 1(a)]. After the geometry optimization, Ni atoms around the vacancy site relax *inward* by 0.06 Å, a pattern opposite to the case of V_{Ni}. This can be understood by the spatial distribution of defect levels, as detailed below. In Fig. 3(c), DOS in the presence of one oxygen vacancy is shown. Three impurity levels are noticeable within the energy gap; one deep level holding two electrons is located at 1 eV above the valence top and two empty levels are found at 0.3 eV below the conduction edge. All three states are dominantly Ni e_g characters in the minority spin direction. This means that the defect levels are derived from the conduction band (see Fig. 2). The occupation of electrons in the minority spin direction reduces the mag-

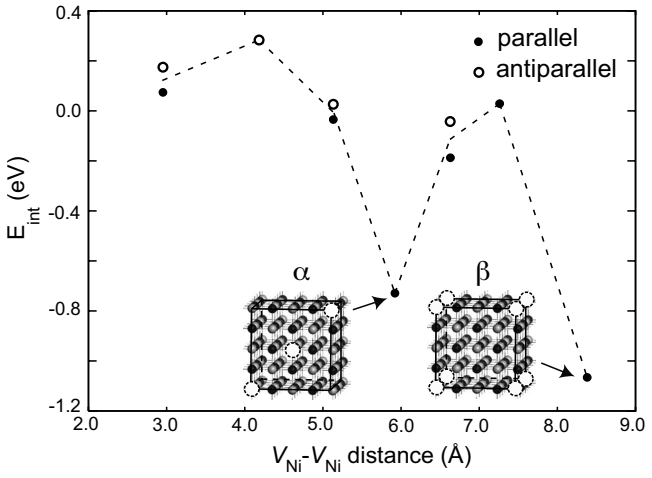

FIG. 5. The V_{Ni}-V_{Ni} interaction energy (E_{int}) with respect to distance. The energy zero is set to the value when two defects are infinitely away. Filled and empty circles indicate data when spin directions of two removed Ni atoms are parallel and antiparallel, respectively. The dashed line is a guide to the eye. In the inset, the defect (blank circles) arrangements for most stable configurations are displayed for a cubic part of the supercell. (The actual computations are done with 128-atom supercells.)

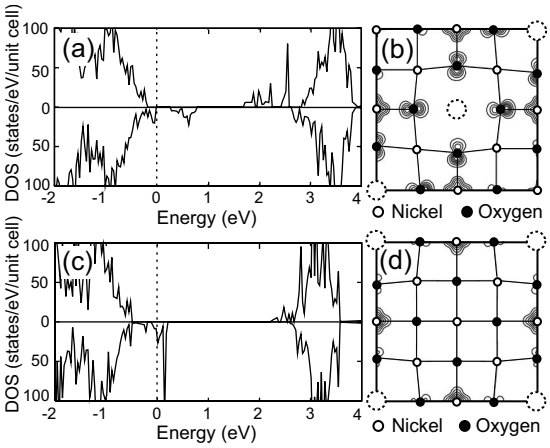

FIG. 6. (a) The density of states for the α configuration in Fig. 5. The Fermi level is set to zero. (b) The squared wave function for a state at the Fermi level in (a) is projected on a plane including paired vacancies (dashed circles). This plane is the front face of the cubic model in Fig. 5. (c) and (d) are similar plots for the β configuration. In (b) and (d), the e_g character at Ni atoms connecting vacancies are noticeably enhanced.

netic moments of Ni atoms to $1.57\mu_B$ from the bulk value of $1.67\mu_B$ (see Table I), a similar effect to the case of V_{Ni}. It is interesting that both V_{Ni} and V_O reduce the magnetic moments of nearby Ni atoms although the microscopic origins are not correlated. The difference between deep and shallow levels lies in the phase relation between six Ni e_g orbitals surrounding the vacancy site. For the deep level, the wave functions are in phase while for the shallow level, they are out of phase, as evidenced in nodal structures between orbitals. These can be interpreted as bonding and antibonding natures, respectively. The bonding character of the occupied deep level is enhanced if Ni atoms relax toward the vacancy site. This would be the main reason for the small inward relaxations mentioned above. The highly localized nature of defect states implies that the presence of the oxygen vacancy in NiO could be confirmed with the luminescence experiment similarly to F centers in ionic crystals.

C. V_{Ni}-V_{Ni} interaction

In order to investigate the interaction between cation vacancies, we remove two Ni atoms with various relative positions within the 128-atom supercell and relax atomic positions. The interaction energy (E_{int}) is evaluated with respect to the reference configuration where two vacancies are infinitely away, as formulated in the following equation:

$$E_{int} = E_{tot}(2V_{Ni}) + E_{tot}(0V_{Ni}) - 2E_{tot}(1V_{Ni}), \qquad (1)$$

where E_{tot} is the total energy of the supercell, including as many nickel vacancies (V_{Ni}) as the number given in the parentheses. Figure 5 shows computed interaction energies for all possible positions in the 128-atom supercell. The most notable thing in Fig. 5 is that two configurations, denoted as α and β, are substantially lower in energy than the others. The defect positions in these geometries are shown as insets in the figure. (For visual clarity, only part of the supercell is drawn.) Figure 6 displays DOS and wave functions at the valence top for α and β. The DOS for α [Fig. 6(a)] indicates an insulating property with a small gap opening of 0.2 eV. On the other hand, DOS for β shows a half-metallic character [see Fig. 6(c)]. We note that nickel vacancies in the β configuration form a simple-cubic lattice, and the model system is, in fact, identical to the case of single V_{Ni} in the 64-atom supercell in Fig. 1(a). The same structure was investigated in Ref. 5 using the SIC method, and a half-metallic property was also noted. However, structural relaxation was not considered in that work, and the choice of stoichiometry was rather arbitrary. Our results provide additional information that the β configuration leading to a half-metallicity is energetically favored as well. This means that when the defect density is sufficiently high, nickel vacancies may condense into a cubic pattern to produce half-metallic domains.

It would be worth examining whether the defect clustering depends on the choice of U. For this, we compare the energy difference between the first and seventh NN positions (the most stable one) as a function of U. The computational results show that relative energies change only by 0.04 and −0.09 eV as reducing or increasing U by 1 eV, respectively (J is fixed). This little affects the energetics in Fig. 5. Therefore, the tendency toward clustering is likely to be a real effect and could be verified experimentally. The insensitivity of interaction energies also implies that the results would not be an artifact of the LDA+U method.

We point out that spatial distributions of defect states play a key role in stabilizing α and β configurations. As observed in Fig. 4(a), the wave functions corresponding to defect levels are weighted at Ni and O atoms along bonding directions. Therefore, they overlap substantially at certain Ni atoms in α and β configurations. This is verified in Figs. 6(b) and 6(d),

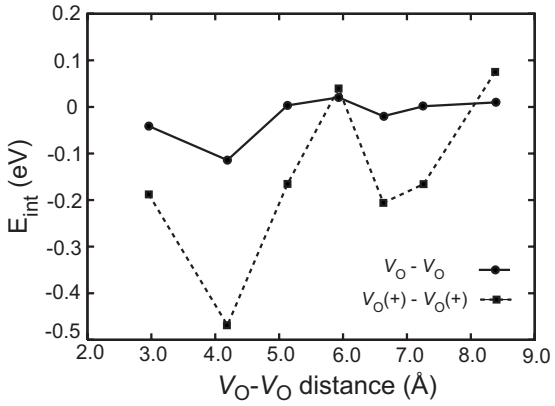

FIG. 7. The interaction energy between two oxygen vacancies. The oxygen vacancies are neutral (V_O) and singly ionized [$V_O(+)$].

which display states at the valence top for α and β, respectively. It can be seen that the e_g character at Ni atoms connecting vacancies are significantly enhanced compared to the single vacancy in Fig. 4(a), and the weights at those Ni atoms are comparable to or even bigger than those of O p orbitals. In passing, we note that there are pairs existing at smaller separations with defect states overlapping at O atoms. However, spin directions are opposite in that case, and the defect states do not couple to each other. We also add that vacancies are multiply bonded in α and β configurations, and the interaction energy in Eq. (1) might be divided by the number of bonds per supercell to conform to the definition. This leads to interaction energies per each pair of Ni vacancies of around −0.4 and −0.2 eV for α and β configurations, respectively.

In order to investigate the role of the lattice in mediating the interactions, we examine the relaxation energies calculated by the energy difference between relaxed and unrelaxed supercells. These energies are −1.92, −1.70, −1.81, −2.15 (α), −1.81, −1.81, and −2.25 (β) eV for configurations with the increasing order of V_{Ni}-V_{Ni} separations (see Fig. 5). Therefore, the clustering of Ni vacancies is well correlated with the relaxation energy of the lattice. The inspection of DOS for the unrelaxed lattices for the α and β configurations indicates that DOS is similar to that for the isolated single vacancy in Fig. 3(b), meaning that defect states are not split much. Therefore, the lattice relaxation effectively enhances the wave function overlap between defect levels, thereby lowering energies for α and β configurations.

D. V_O-V_O interaction

Next, we calculate the interaction energy between two oxygen vacancies in a similar manner to nickel vacancies, using 128-atom supercells. The results are shown in Fig. 7. Depending on the spin direction of nearby Ni atoms, there are two nonequivalent configurations for some V_O-V_O separations. However, computed energy differences are negligibly small (0.01 eV at the first NN position), and only one of them is displayed in Fig. 7. Compared to cation vacancies, the interactions between oxygen vacancies are relatively weak with a minimum E_{int} of −0.1 eV. When oxygen vacancies are close to each other, defect states overlap and energy levels are split due to bonding or antibonding combinations of wave functions. However, changes in the total energy are small because those states are already fully occupied. This is contrasted to the case of nickel vacancies where defect levels are partially occupied, and substantial energy gain is achieved by occupying only defect levels with a bonding character. However, the results change drastically when oxygen vacancies are partially ionized; by reducing the total number of electrons within the supercell by 2, one can compute interaction energies between two singly ionized vacancies [$V_O(+)$] as in the following:

$$E_{int} = E_{tot}(2V_O;+2) + E_{tot}(0V_O;+0) - 2E_{tot}(1V_O;+1), \quad (2)$$

where $+n$ indicates the charge state of the supercell.[33,34] The negative jellium charges are introduced to compensate for the positive charges in Eq. (2). The computed interaction energies are shown in Fig. 7. It is interesting that most interaction energies for the charged defects are negative although repulsive electrostatic interactions are expected between defects or dopants with same charge states.[34] In particular, it is noted that the stability of V_O's at the second NN position is greatly enhanced. A detailed analysis will be given below. Since the charged defects are repeated under three-dimensional periodic boundary conditions, the spurious electrostatic interactions might influence the binding energies. In order to confirm that the computed results are well converged with respect to the supercell size, we carry out additional calculations with a larger supercell including 192 atoms constructed by expanding the conventional cell of NiO with a hexagonal symmetry. The unit cell lengths of supercells are a=11.85 Å and c=14.52 Å. This supercell is 50% larger than the one used in Fig. 7. We calculate the interaction energy for the most stable geometry (second NN pair) based on Eq. (2) and find that the interaction energy changes by less than 3% (from −0.472 to −0.485 eV). This reflects that the interaction energies presented in Fig. 7 are well converged with respect to the supercell size, especially those for small separations.

In order to enlighten the microscopic origin of V_O-V_O interactions, we first examine relaxation energies for each configuration. They are −0.47, −0.39 (most stable), −0.41, −0.28, −0.43, −0.41, and −0.31 eV for configurations in Fig. 7 with the increasing order of defect separations. Compared to Ni vacancies discussed above, the relaxation energies are much smaller, and they are not correlated to the stability of paired vacancies. Next, we inspect DOS as well as squared wave functions for neutral oxygen vacancies. In Fig. 8(a), DOS for the first NN pair is drawn. It can be seen that energy levels of defect states are split by 0.2 eV due to the overlap of wave functions. The energy splitting is rather small because two Ni e_g orbitals that originate from different V_O's are orthogonal to each other [see Fig. 8(c)]. On the other hand, for second NN pairs of V_O, only one Ni atom is shared, but the orbital shape is common for two defect states [see Fig. 8(d)]. This increases the overlap integral at the Ni site, and the energy splitting in the down-spin direction is as much as

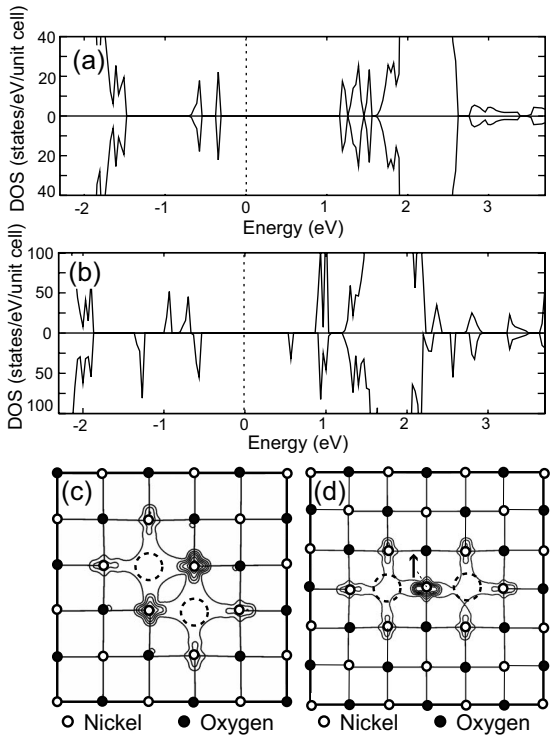

FIG. 8. Total density of states for (a) first NN and (b) second NN pairs of neutral oxygen vacancies. The Fermi level is denoted by vertical dotted lines. (c) and (d) show squared wave functions of highest occupied states, added over spin directions. The arrow in (d) denotes the majority spin direction at the overlapping Ni site.

0.8 eV, as shown in Fig. 8(b). In constrast, the defect levels in the up-spin direction are split much less. As shown in Fig. 8(d), two V_O's are connected to Ni atoms with the up-spin direction. As discussed in Sec. III B 2, the defect states are derived from the conduction band with a minority spin direction of host Ni atoms. Therefore, the maximum overlap occurs for the down-spin direction since the overlapping Ni atom is in the up-spin direction. The large energy splitting explains why charged defects show a strong tendency toward pairing at the second NN position; as defect clusters are disposed of two electrons, only high-lying states of the antibonding character are emptied. Therefore, configurations showing a large splitting of the defect levels are energetically favored among charged defects. This also indicates that the maximum interaction energy will be achieved when two V_O's are singly ionized. For example, if only one electron is removed from the supercell, imitating interaction between $V_O(+)$ and V_O, the magnitude of the interaction energy of second NN pairs is reduced by 0.1 eV. The generality of the above discussion implies that the attractive interactions between charged oxygen vacancies could apply to other oxides as well. In fact, we find a similar behavior in Al_2O_3.[35]

IV. SUMMARY

In summary, we studied electronic properties of NiO including vacancy defects using the LDA+U method. In the case of the nickel vacancy, we identified bound hole states extending over approximately 4 Å from the vacancy site with the binding energy of 0.2 eV. On the other hand, the oxygen vacancy creates defect levels within the energy gap similar to F centers in ionic crystals. The interactions between vacancies were consistently explained based on the overlap of defect states. It was found that nickel vacancies could be ordered in a simple-cubic pattern, leading to a half-metallic property. In the case of oxygen vacancies, the relative position sharing one Ni atom was most favored with its stability greatly enhanced when defects are singly ionized. For both nickel and oxygen vacancies, the partial occupation of defect states was important to enhance the tendency toward defect ordering or clustering.

ACKNOWLEDGMENTS

The work was supported by the National Program for 0.1 Terabit NVM Devices, the Korea Science and Engineering Foundation through the Basic Research program (Grant No. R01-2006-000-10883-0), and Samsung Electronics. The computations were carried out at Korea Institute of Science and Technology Information (KISTI) through the seventh Strategic Supercomputing Program.

*Corresponding author: hansw@ewha.ac.kr

[1] P. A. Cox, *Transition Metal Oxides: An Introduction to Their Electronic Structure and Properties*, The International Series of Monographs on Chemistry Vol. 27 (Clarendon, Oxford, 1995).
[2] D. I. Woodward, I. M. Reaney, G. Y. Yang, E. C. Dickey, and C. A. Randall, Appl. Phys. Lett. **84**, 4650 (2004).
[3] D. A. Muller, N. Nakagawa, A. Ohtomo, J. L. Grazul, and H. Y. Hwang, Nature (London) **430**, 657 (2004).
[4] K. Terakura, T. Oguchi, A. R. Williams, and J. Kübler, Phys. Rev. B **30**, 4734 (1984).
[5] D. Ködderitzsch, W. Hergert, Z. Szotek, and W. M. Temmerman, Phys. Rev. B **68**, 125114 (2003).
[6] S. Seo, M. J. Lee, D. H. Seo, E. J. Jeoung, D.-S. Suh, Y. S. Joung, I. K. Yoo, I. R. Hwang, S. H. Kim, I. S. Byun, J.-S. Kim, J. S. Choi, and B. H. Park, Appl. Phys. Lett. **85**, 5655 (2004).
[7] S. H. Jeon, B. Park, J. Lee, B. Lee, and S. Han, Appl. Phys. Lett. **89**, 042904 (2006).
[8] S. V. Faleev, M. van Schilfgaarde, and T. Kotani, Phys. Rev. Lett. **93**, 126406 (2004).
[9] D. Ködderitzsch, W. Hergert, W. M. Temmerman, Z. Szotek, A. Ernst, and H. Winter, Phys. Rev. B **66**, 064434 (2002).
[10] A. Filippetti and N. A. Spaldin, Phys. Rev. B **67**, 125109 (2003).
[11] M. D. Towler, N. L. Allan, N. M. Harrison, V. R. Saunders, W. C. Mackrodt, and E. Aprà, Phys. Rev. B **50**, 5041 (1994).
[12] G. Lefkidis and W. Hübner, Phys. Rev. Lett. **95**, 077401 (2005).
[13] C. de Graaf, F. Illas, R. Broer, and W. C. Nieuwpoort, J. Chem. Phys. **106**, 3287 (1997).
[14] T. Bredow and A. R. Gerson, Phys. Rev. B **61**, 5194 (2000).

[15] S. L. Dudarev, G. A. Botton, S. Y. Savrasov, C. J. Humphreys, and A. P. Sutton, Phys. Rev. B **57**, 1505 (1998).
[16] O. Bengone, M. Alouani, P. Blöchl, and J. Hugel, Phys. Rev. B **62**, 16392 (2000).
[17] A. Rohrbach, J. Hafner, and G. Kresse, Phys. Rev. B **69**, 075413 (2004).
[18] M. R. Castell, S. L. Dudarev, G. A. D. Briggs, and A. P. Sutton, Phys. Rev. B **59**, 7342 (1999).
[19] G. Kresse and J. Hafner, Phys. Rev. B **47**, 558(R) (1993); **49**, 14251 (1994).
[20] P. E. Blöchl, Phys. Rev. B **50**, 17953 (1994).
[21] J. P. Perdew, K. Burke, and M. Ernzerhof, Phys. Rev. Lett. **77**, 3865 (1996).
[22] V. I. Anisimov, J. Zaanen, and O. K. Andersen, Phys. Rev. B **44**, 943 (1991).
[23] M. Cococcioni and S. de Gironcoli, Phys. Rev. B **71**, 035105 (2005).
[24] R. W. G. Wyckoff, *Crystal Structures* (Interscience, New York, 1964).
[25] A. K. Cheetham and D. A. O. Hope, Phys. Rev. B **27**, 6964 (1983).
[26] R. J. Powell and W. E. Spicer, Phys. Rev. B **2**, 2182 (1970).
[27] D. Adler and J. Feinleib, Phys. Rev. B **2**, 3112 (1970).
[28] J. McNatt, Phys. Rev. Lett. **23**, 915 (1969).
[29] S. Hüfner and T. Riesterer, Phys. Rev. B **33**, 7267 (1986).
[30] M. R. Castell, P. L. Wincott, N. G. Condon, C. Muggelberg, G. Thornton, S. L. Dudarev, A. P. Sutton, and G. A. D. Briggs, Phys. Rev. B **55**, 7859 (1997).
[31] S. L. Dudarev, A. I. Liechtenstein, M. R. Castell, G. A. D. Briggs, and A. P. Sutton, Phys. Rev. B **56**, 4900 (1997).
[32] P. Lunkenheimer, A. Loidl, C. R. Ottermann, and K. Bange, Phys. Rev. B **44**, 5927 (1991).
[33] S. Limpijumnong, S. B. Zhang, S.-H. Wei, and C. H. Park, Phys. Rev. Lett. **92**, 155504 (2004).
[34] Y.-S. Kim, E.-C. Lee, and K. J. Chang, Phys. Rev. Lett. **91**, 125503 (2003).
[35] C.-K. Lee, S. H. Jeon, B. H. Park, and S. Han (unpublished).